Magnetospheric chaos and dynamical complexity response during storm time disturbance

Irewola Aaron Oludehinwa[1], Olasunkanmi Isaac Olusola[1], Olawale Segun Bolaji[1,2], Olumide Olayinka Odeyemi[1], Abdullahi Ndzi Njah[1]

[1]Department of Physics, University of Lagos, Nigeria

[2]Department of Physics, University of Tasmania, Australia

Abstract

In this study, we examine the magnetospheric chaos and dynamical complexity response to the disturbance storm time (D_{st}) and solar wind electric field (VB_s) during different categories of geomagnetic storm (minor, moderate and major geomagnetic storm). The time series data of the D_{st} and VB_s are analyzed for the period of nine years using nonlinear dynamics tools (Maximal Lyapunov Exponent, MLE, Approximate Entropy, ApEn and Delay Vector Variance, DVV). We found a significant trend between each nonlinear parameter and the categories of geomagnetic storm. The MLE and ApEn values of the D_{st} indicate that chaotic and dynamical complexity responses are high during minor geomagnetic storms, reduce at moderate geomagnetic storms and decline further during major geomagnetic storms. However, the MLE and ApEn values obtained from VB_s indicate that chaotic and dynamical complexity responses are high with no significant difference between the periods that are associated with minor, moderate and major geomagnetic storms. The test for nonlinearity in the D_{st} time series during major geomagnetic storm reveals the strongest nonlinearity features. Based on these findings, the dynamical features obtained in the VB_s as input and D_{st} as output of the magnetospheric system suggest that the magnetospheric dynamics is nonlinear and the solar wind dynamics is consistently stochastic in nature.

Keywords: D_{st} signals, Solar wind electric field (VB_s) signals, Geomagnetic storm, Chaotic behaviour, Dynamical complexity, Nonlinearity.

1.0 Introduction

The response of chaos and dynamical complexity behaviour with respect to magnetospheric dynamics varies (Tsurutani et al., 1990). This is due to changes in the interplanetary electric fields imposed on the magnetopause and those penetrating the inner magnetosphere and sustaining convection thereby initiating geomagnetic storm (Dungey, 1961; Pavlos et al., 1992). A prolonged southward turning of interplanetary magnetic field (IMF,B_z), which indicates that solar wind-magnetosphere coupling is in-progress was confirmed on many occasions for which such geomagnetic storm was driven by Corotating Interaction Regions (CIRs), or by the sheath preceding an interplanetary coronal mass ejection (ICME) or by a combination of the sheath and an ICME magnetic cloud (Gonzalez and Tsurutani, 1987; Tsurutani and Gonzalez, 1987; Tsurutani et al., 1988; Cowley, 1995; Tsutomu, 2002; Yurchyshyn et al., 2004; Kozyra et al., 2006; Echer et al., 2008; Meng et al., 2019; Tsurutani et al., 2020). The sporadic magnetic reconnection between the southward component of the Alfven waves and the earth's magnetopause leads to isolated substorms/convention events such as the high intensity long-duration continuous AE activity (HILDCAA) which are shown to last from days to weeks (Akasofu, 1964; Tsurutani and Gonzalez, 1987; Hajra et al., 2013; Liou et al., 2013; Mendes et al., 2017; Hajra and Tsurutani, 2018; Tsurutani and Hajra, 2021). Notably, the introduction of Disturbance Storm Time (D_{st}) index (Sugiura, 1964; Sugiura and Kamei, 1991) unveiled the quantitative measure of the total energy of the ring current particles. Therefore, the D_{st} index remains one of the most popular global indicators that can precisely reveal the severity of a geomagnetic storm (Dessler and Parker, 1959).

The D_{st} fluctuations exhibit different signatures for different categories of geomagnetic storm. Ordinarily, one can easily anticipate that fluctuations in a D_{st} signal appear chaotic and complex.

48 These may arise from the changes in the interplanetary electric fields driven by the solar wind-

49 magnetospheric coupling processes. At different categories of geomagnetic storm, fluctuations in

50 the D_{st} signals differ (Oludehinwa et al., 2018). One obvious reason is that as the intensity of the

51 geomagnetic storm increases, the fluctuation behaviour in the D_{st} signal becomes more complex

52 and nonlinear in nature. It has been established that the electrodynamic response of the

53 magnetosphere to solar wind drivers are non-autonomous in nature (Price and Prichard, 1993;

54 Price et al., 1994; Johnson and Wings, 2005). Therefore, the chaotic analysis of the

55 magnetospheric time series must be related to the concept of input-output dynamical process

56 (Russell et al., 1974; Burton et al.,1975; Gonzalez et al., 1989; Gonzalez et al., 1994).

57 Consequently, it is necessary to examine the chaotic behaviour of the solar wind electric field

58 (VB_s) as input signals and the magnetospheric activity index (D_{st}) as output during different

59 categories of geomagnetic storms.

60 Several works have been presented on the chaotic and dynamical complexity behaviour of the

61 magnetospheric dynamics based on autonomous concept, i.e using the time series data of

62 magnetospheric activity alone such as auroral electrojet (AE), Amplitude Lower (AL) and D_{st}

63 index (Vassiliadis et al.,1990; Baker and Klimas, 1990; Vassiliadis et al.,1991; Shan et al., 1991;

64 Pavlos et al., 1994; Klimas et al., 1996; Valdivia et al., 2005; Mendes et al., 2017; Consolini,

65 2018). They found evidence of low-dimensional chaos in the magnetospheric dynamics. For

66 instance, the report by Vassiliadis et al. (1991) shows that the computation of Lyapunov exponent

67 for AL index time series gives a positive value of Lyapunov exponent indicating the presence of

68 chaos in the magnetospheric dynamics. Unnikrishnan, (2008) studied the deterministic chaotic

69 behaviour in the magnetospheric dynamics under various physical conditions using AE index time

70 series and found that the seasonal mean value of Lyapunov exponent in winter season during quiet

71   periods $(0.7 \pm 0.11\ min^{-1})$ is higher than that of the stormy periods $(0.36 \pm 0.09\ min^{-1})$.

72   Balasis et al. (2006) examined the magnetospheric dynamics in the D_{st} index time series from

73   pre-magnetic storm to magnetic storm period using fractal dynamics. They found that the transition

74   from anti-persistent to persistent behaviour indicates that the occurrence of an intense geomagnetic

75   storm is imminent. Balasis et al. (2009) further reveal the dynamical complexity behaviour in the

76   magnetospheric dynamics using various entropy measures. They reported a significant decrease in

77   dynamical complexity and an accession of persistency in the D_{st} time series as the magnetic storm

78   approaches. Recently, Oludehinwa et al. (2018) examined the nonlinearity effects in D_{st} signals

79   during minor, moderate and major geomagnetic storm using recurrence plots and recurrence

80   quantification analyses. They found that the dynamics of the D_{st} signal is stochastic during minor

81   geomagnetic storm periods and deterministic as the geomagnetic storm increases.

82   Also, studies describing the solar wind and magnetosphere as a non-autonomous system have been

83   extensively investigated. Price et al. (1994) examine the nonlinear input-output analysis of AL

84   index and different combinations of interplanetary magnetic field (IMF) with solar wind

85   parameters as input functions. They found that only a few of the input combinations show any

86   evidence whatsoever for nonlinear coupling between the input and output for the interval

87   investigated. Pavlos et al. (1999) presented further evidence of magnetospheric chaos. They

88   compared the observational behaviour of the magnetospheric system with the results obtained by

89   analyzing different types of stochastic and deterministic input-output systems and asserted that a

90   low dimensional chaos is evident in magnetospheric dynamics. Devi et al. (2013) studied the

91   magnetospheric dynamics using AL index and the southward component of IMF(B_z). They

92   observed that the magnetosphere and turbulent solar wind have values corresponding to nonlinear

93   dynamical system with chaotic behaviour. The modeling and forecasting approach have been

94   applied to magnetospheric time series using nonlinear models (Valdivia et al., 1996; Vassiliadis et

95   al., 1999; Vassiliadis, 2006; Balikhin et al., 2010). These efforts have improved our understanding

96   that the concept of nonlinear dynamics can reveal some hidden dynamical information in the

97   observational time series. In addition to these nonlinear effects in D_{st} signals, a measure of the

98   exponential divergence and convergence within the trajectories of a phase space known as

99   Maximal Lyapunov Exponent (MLE), which has the potential to depict the chaotic behavior in the

100   D_{st} and VB_s time series during a minor, moderate and major geomagnetic storm have not been

101   investigated. In addition, to the best of our knowledge, computation of Approximate Entropy

102   (ApEn) that depicts the dynamical complexity behaviour during different categories of

103   geomagnetic storm has not been reported in the literature. The test for nonlinearity through delay

104   vector variance (DVV) analysis that reveals the nonlinearity features in D_{st} and VB_s time series

105   during minor, moderate and major geomagnetic storms is not well known. It is worth to note that

106   understanding the dynamical characteristics in the D_{st} and VB_s signals at different categories of

107   geomagnetic storms will provide useful diagnostic information to different conditions of space

108   weather phenomenon. Consequently, this study attempts to carry out comprehensive numerical

109   analyses to unfold the chaotic and dynamical complexity behaviour in the D_{st} and VB_s signals

110   during minor, moderate and major geomagnetic storm. In section 2, our methods of data

111   acquisition are described. Also, the nonlinear analysis that we employed in this investigation are

112   detailed. In section 3, we unveiled our results and engage the discussion of results in section 4.

113   **2.0 Description of the Data and Nonlinear Dynamics**

114   The D_{st} index is derived by measurements from ground-based magnetic stations at low-latitudes

115   observatories around the world and depicts mainly the variation of the ring current, as well as the

116   Chapman-Ferraro Magnetopause currents, and tail currents to a lesser extent (Sugiura, 1964;

117 Feldstein et al., 2005; Feldstein et al., 2006; Love and Gannon, 2009). Due to its global nature, D_{st}

118 time series provides a measure of how intense a geomagnetic storm was (Dessel and Parker, 1959).

119 In this study, we considered D_{st} data for the period of nine years from January to December

120 between 2008 and 2016 which were downloaded from the World Data Centre for Geomagnetism,

121 Kyoto, Japan (http://wdc.kugi-kyoto-u.ac.jp/Dstae/index.html). We use the classification of

122 geomagnetic storms as proposed by Gonzalez et al. (1994) such that D_{st} index value in the ranges

123 $0 \leq Dst \leq -50nT$, $-50nT \leq Dst \leq -100nT$, $-100nT \leq Dst \leq -250nT$ are classified as

124 minor, moderate and major geomagnetic storms respectively and each time series is being

125 classified based on its minimum D_{st} value. The solar wind electric field (VB_s) data are archived

126 from the National Aeronautics and Space Administration, Space Physics Facility

127 (http://omniweb.gsfc.nasa.gov). The sampling time of D_{st} and VB_s time series data was 1-hour. It

128 is well known that the dynamics of the solar wind contribute to the driving of the magnetosphere

129 (Burton et al. 1975). Furthermore, we took the solar wind electric field (VB_s) as the input signal

130 (Price and Prichard, 1993; Price et al., 1994). The VB_s was categorized according to the periods

131 of minor, moderate and major geomagnetic storm. Then, the D_{st} and VB_s time series were

132 subjected to a variety of nonlinear analytical tools explained as follow:

133 **2.1 Phase Space Reconstruction and Observational time series**

134 An observational time series can be defined as a sequence of scalar measurements of some

135 quantity, which is a function of the current state of the system taken at multiples of a fixed sampling

136 time. In nonlinear dynamics, the first step in analyzing an observational time series data is to

137 reconstruct an appropriate state space of the system. Takens (1981) and Mane (1981) stated that

138 one time series or a few simultaneous time series are converted to a sequence of vectors. This

139   reconstructed phase space has all the dynamical characteristic of the real phase space provided the

140   time delay and embedding dimension are properly specified.

141    $$X(t) = [x(t), x(t + \tau), x(t + 2\tau), \dots, x(t + (m - 1)\tau]^T \qquad (1)$$

142   Where $X(t)$ is the reconstructed phase space, $x(t)$ is the original time series data, τ is the time

143   delay and m is the embedding dimension. An appropriate choice of τ and m are needed for the

144   reconstruction of phase space which is determined by average mutual information and false nearest

145   neighbor, respectively.

146   **2.2 Average Mutual Information (AMI)**

147   The method of Average Mutual Information (AMI) is one of the nonlinear techniques used to

148   determine the optimal time delay (τ) required for phase space reconstruction in observational time

149   series. The time delay mutual information was proposed by Fraser and Swinney, (1986) instead of

150   an autocorrelation function. This method takes into account nonlinear correlations within the time

151   series data. It measures how much information can be predicted about one time series point, given

152   full information about the other. For instance, the mutual information between x_i and $x_{(i+\tau)}$

153   quantifies the information in state $x_{(i+\tau)}$ under the assumption that information at the state x_i is

154   known. The AMI for a time series, $x(t_i), \quad i = 1,2, \dots, N$ is calculated as:

155    $$I(T) = \sum_{x(t_i),\ x(t_i+T)} P(x(t_i), x(t_i + T)) \times \log_2 \left[\frac{P(x(t_i), x(t_i+T))}{P(x(t_i))\, P(x(t_i+T))} \right] \qquad (2)$$

156   where $x(t_i)$ is the ith element of the time series, $T = k\Delta t \ \ (k = 1,2, \dots, k_{max})$, $P(x(t_i))$ is the

157   probability density at $x(t_i)$, $P(x(t_i), x(t_i + T))$ is the joint probability density at the pair

158    $x(t_i), x(t_i + T)$. The time delay (τ) of the first minimum of AMI is chosen as optimal time delay

159   (Fraser and Swinney, 1986). Therefore, the AMI was applied to the D_{st} and VB_s time series and

160   the plot of AMI versus time delay is shown in Figure (3). We notice that the AMI showed the first

161   local minimum at roughly $\tau = 15hr$. Furthermore, the values of τ near this value of ~15hr

162   maintain constancy for both VB_s and D_{st}. In the analysis $\tau = 15hr$ was used as the optimal time

163   delay for the computation of maximal Lyapunov exponent.

164   **2.3 False Nearest Neighbor (FNN)**

165   In determining the optimal choice of embedding dimension(m), the false nearest neighbor method

166   was used in the study. The method was suggested by Kennel et al. (1992). The concept is based

167   on how the number of neighbors of a point along a signal trajectory changes with increasing

168   embedding dimension. With increasing embedding dimension, the false neighbor will no longer

169   be neighbors, therefore by examining how the number of neighbors changes as a function of

170   dimension, an appropriate embedding dimension can be determined. For instance, suppose we

171   have a one-dimensional time series. We can construct a time series $y(t)$ of D-dimensional points

172   from the original one-dimensional time series $x(t)$ as follows:

173 $$y(t) = (x(t), x(t + \tau), \dots, x(t + (D - 1)\tau)) \qquad (3)$$

174   where τ and D are time delay and embedding dimension. Using the formular from Kennel et al.

175   (1992); Wallot and Monster, (2018), if we have a D-dimensional phase space and denote the rth

176   nearest neighbor of a coordinate vector $y(t)$ by $y^{(r)}(t)$, then the square of the Euclidean distance

177   between $y(t)$ and the rth nearest neighbor is:

178 $$R_D^2(t, r) = \sum_{k=0}^{D-1} \left[x(t + k\tau) - x^{(r)}(t + k\tau) \right]^2 \qquad (4)$$

179   Now applying the logic outlined above, we can go from a D-dimensional phase space to $(D + 1)$

180   dimensional phase space by time-delay embedding, adding a new coordinate to $y(t)$, and ask what

181   is the squared distance between $y(t)$ and the same rth nearest neighbor:

182   $$R_{D+1}^2(t,r) = R_D^2(t,r) + \left[x(t + D\tau) - x^{(r)}(t + D\tau)\right]^2 \qquad (5)$$

183   As explained above, if the one-dimensional time series is already properly embedded in D

184   dimensions, then the distance R between $y(t)$ and the rth nearest neighbor should not change

185   appreciably by some distance criterion $R_{tol}(i.e\ R < R_{tol})$. Moreover, the distance of the nearest

186   neighbor when embedded into the next higher dimension relative to the size of the attractor should

187   be less than some criterion $A_{tol}(i.e\ R_{D+1} < A_{tol})$. Doing this for the nearest neighbor of each

188   coordinate will result on many false nearest neighbors when embedding is insufficient or in few

189   (or no) false neighbors when embedding is sufficient. In the analysis, the FNN was applied to the

190   D_{st} and VB_s time series to detect the optimal value of embedding dimension(m). Figure (4) shows

191   a sample plot of the percentage of false nearest neighbor against embedding dimension in one of

192   the months under investigation (other months show similar results, thus for brevity we depict only

193   one of the results). We notice that the false nearest neighbor attains its minimum value at $m \geq 5$

194   indicating that embedding dimension (m) from $m \geq 5$ are optimal values. Therefore, $m = 5$ was

195   used for the computation of maximal Lyapunov exponent.

196   **2.4 Maximal Lyapunov Exponent (MLE)**

197   The Maximal Lyapunov Exponent (MLE) is one of the most popular nonlinear dynamics tool used

198   for detecting chaotic behaviour in a time series data. It describes how small changes in the state of

199   a system grow at an exponential rate and eventually dominate the behaviour. An important

200   indication of chaotic behavior of a dissipative deterministic system is the existence of a positive

201 Lyapunov Exponent. A positive MLE signifies divergence of trajectories in one direction or

202 expansion of an initial volume in this direction. On the other hand, a negative MLE exponent

203 implies convergence of trajectories or contraction of volume along another direction. The

204 algorithm proposed by Wolf et al. (1985) for estimating MLE is employed to compute the chaotic

205 behavior of the D_{st} and VB_s time series at minor, moderate and major geomagnetic storm. Other

206 methods of determining MLE includes Rosenstein's method, Kantz's method and so on. In this

207 study, the MLE at minor, moderate and major geomagnetic storms periods was computed with

208 $m = 5$ and $\tau = 15hr$ as shown in figures (5 & 6-bar plots) for D_{st} and VB_s. The calculation of

209 MLE is explained as follows: given a sequence of vector $x(t)$, an m-dimensional phase space is

210 formed from the observational time series through embedding theorem as

211
$$\{x(t), x(t + \tau), \dots, x(t + (m - 1)\tau)\} \tag{6}$$

212 where m and τ are as defined earlier, after reconstructing the observational time series, the

213 algorithm locates the nearest neighbor (in Euclidean sense) to the initial point $\{x(t_0), \dots, x(t_0 + $

214 $(m - 1)\tau\}$ and denote the distance between these two points $L(t_0)$. At a later point t_1, the initial

215 length will have evolved to length $L'(t_1)$. Then the MLE is calculated as:

216
$$\lambda = \frac{1}{t_M - t_0} \sum_{k=1}^{M} \log_2 \frac{L'(t_k)}{L(t_{k-1})} \tag{7}$$

217 M is the total number of replacement steps. We look for a new data point that satisfies two criteria

218 reasonably well: its separation, $L(t_1)$, from the evolved fiducial point is small. If an adequate

219 replacement point cannot be found, we retain the points that were being used. This procedure is

220 repeated until the fiducial trajectory has traversed the entire data.

221

222 **2.5 Approximate Entropy (ApEn)**

223 Approximate Entropy (ApEn) is one of the nonlinear dynamics tools that measure the dynamical

224 complexity in observational time series. The concept was proposed by Pincus, (1991) which

225 provides a generalized measure of regularity, such that it accounts for the logarithm likelihood in

226 the observational time series. For instance, a dataset of length, N, that repeat itself for m points

227 within a boundary will again repeat itself for $m + 1$ points. Because of its computational

228 advantage, ApEn has been widely used in many areas of disciplines to study dynamical complexity

229 (Pincus and Kalman (2004); Pincus and Goldberger (1994); McKinley et al. (2011); Kannathan et

230 al. (2005); Balasis et al. (2009); Shujuan and Weidong, (2010); Moore and Marchant (2017)). The

231 ApEn is computed using the formula below:

232 $$ApEn(m,r,N) = \frac{1}{N-m+1}\sum_{i=1}^{N-m+1}\log C_i^m(r) - \frac{1}{N-m}\sum_{i=1}^{N-m}\log C_i^m(r) \qquad (8)$$

233 where $C_i^m(r) = \frac{1}{N-m+1}\sum_{j=1}^{N-m+1}\Theta\left(r - \|x_i - x_j\|\right)$ is the correlation integral, m is the embedding

234 dimension and r is the tolerance. To compute the ApEn for the D_{st} and VB_s time series classified

235 as minor, moderate and major geomagnetic storm from 2008 to 2016, we choose $(m = 3, \tau =$

236 $1hr)$. We refer the works of Pincus, (1991); Kannathal et al. (2005); and Balasis et al. (2009) to

237 interested readers where all the computational steps regarding ApEn were explained in details.

238 Figures (5 & 6) depict the stem plot of ApEn for D_{st} and (VB_s) from 2008 to 2016.

239 **2.6 Delay Vector Variance (DVV) analysis**

240 The Delay Vector Variance (DVV) is a unified approach in analyzing and testing for nonlinearity

241 in a time series (Gautama et al., 2004; Mandic et al., 2007). The basic idea of the DVV is that, if

242 two delay vectors of a predictable signal are close to each other in terms of the Euclidean distance,

243   they should have similar target. For instance, when a time delay (τ) is embedded into a time series

244    $x(k),\ k = 1,2,\dots,N$, then a reconstructed phase space vector is formed which represents a set of

245   delay vectors (DVs) of a given dimension.

246    $$X(k) = [X_{k-m\tau},\dots,X_{k-\tau}]^T \tag{9}$$

247   Reconstructing the phase space, a set (λ_k) is generated by grouping those DVs that are with a

248   certain Euclidean distance to DVs $(X(k))$. For a given embedding dimension (m), a measure of

249   unpredictability $\sigma *^2$ is computed over all pairwise Euclidean distance between delay vector as

250    $$d(i,j) = \|x(i) - x(j)\| \quad (i \neq j) \tag{10}$$

251   Then, sets $\lambda_k(r_d)$ are generated as the sets which consist of all delay vectors that lie closer to $x(k)$

252   than a certain distance r_d.

253    $$\lambda_k(r_d) = \{x(i)\|x(k) - x(i)\| \leq r_d\} \tag{11}$$

254   For every set $\lambda_k(r_d)$, the variance of the corresponding target $\sigma *^2 (r_d)$ is

255    $$\sigma *^2 (r_d) = \frac{\frac{1}{N}\sum_{k=1}^{N}\sigma_k^2(r_d)}{\sigma_k} \tag{12}$$

256   where $\sigma *^2 (r_d)$ is target variance against the standardized distance indicating that Euclidean

257   distance will be varied in a manner standardized with respect to the distribution of pairwise

258   distance between DVs. Iterative Amplitude Adjusted Fourier Transform (IAAFT) method is used

259   to generate the surrogate time series (Kugiumtzis, 1999). If the surrogate time series yields DV

260   plots similar to the original time series and the scattered plot coincides with the bisector line, then

261   the original time series can be regarded as linear (Theiler et al., 1992; Gautama et al., 2004; Imitaz,

262   2010; Jaksic et al., 2016). On the other hand, if the surrogate time series yields DV plot that is not

263   similar to that of the original time series, then the deviation from the bisector lines indicates

264   nonlinearity. The deviation from the bisector lines grows as a result of the degree of nonlinearity

265   in the observational time series.

266
$$t^{DVV} = \sqrt{\langle(\sigma^{*2}(r_d) - \frac{\Sigma_{i=1}^{N}\sigma_{s,i}^{*2}}{N_s})\rangle} \qquad (13)$$

267   where $\sigma_{s,i}^{*2}(r_d)$ is the target variance at the span r_d for the ith surrogate. To carry out the test for

268   nonlinearity in the D_{st} signals, $m = 3$ and $n_d = 3$, the number of reference DVs=200, and number

269   of surrogate, $N_s = 25$ was used in all the analysis. Then we examined the nonlinearity response at

270   minor, moderate and major geomagnetic storm.

3.0 Results

In this study, D_{st} and VB_s time series from January to December were analyzed for the period of nine years (2008 to 2016) to examine the chaotic and dynamical complexity response in the magnetospheric dynamics during minor, moderate and major geomagnetic storms. Figures (1) & (2), display the samples of fluctuation signatures of D_{st} and VB_s signals classified as (a): minor, (b): moderate and (c): major geomagnetic storms. The plot of Average Mutual information against time delay (τ) shown in Figure (3) depicts that the first local minimum of the AMI function was found to be roughly at $\tau = 15$hr. Furthermore, we notice that the values of τ near this value of (~15hr) maintain constancy for both VB_s and D_{st}. Also, in Figure (4), we display the plot of the percentage of false nearest neighbor against embedding dimension (m). It is obvious that a decrease in false nearest neighbor when increasing the embedding dimension drop steeply to zero at the optimal dimension($m = 5$), thereafter the false neighbors stabilizes at that $m = 5$ for VB_s and D_{st}. Therefore, $m = 5$ and $\tau = 15$hr was used for the computation of MLE at different categories of geomagnetic storm, while $m = 3$ and $\tau = 1$hr are applied for the computation of ApEn values.

The results of MLE (bar plot) and ApEn (stem plot) for D_{st} at minor, moderate and major geomagnetic storms are shown in Figure 5. During minor geomagnetic storms, we notice that the value of MLE ranges between 0.07 and 0.14 for most of the months classified as minor geomagnetic storm. Similarly, the ApEn (stem plot) ranges between 0.59 and 0.83. It is obvious that strong chaotic behaviour with high dynamical complexity are associated with minor geomagnetic storms. During moderate geomagnetic storms, (see b part of Figure 5), we observe a reduction in MLE values $(0.04 - 0.07)$ compared to minor geomagnetic storm periods. Within the observed values of MLE during moderate geomagnetic storms, we found a slight rise of MLE

294   in the following months (Mar 2008), (Apr 2011), (Jan 2012, Feb 2012, Apr 2012), (Jul 2015, Aug

295   2015, Sept 2015, Oct 2015, Nov 2015) and (Nov 2016). Also, the ApEn revealed a reduction in

296   values between 0.44 and 0.57 during moderate geomagnetic storms. The lowest values of ApEn

297   were noticed in the following months: May 2010, Mar 2011, and Jan 2016. During major

298   geomagnetic storms as shown in Figure 5, the minimum and maximum value of MLE is

299   respectively 0.03 and 0.04 implying a very strong reduction of chaotic behaviour compared with

300   minor and moderate geomagnetic storms. The lowest values of MLE were found in the months of

301   Jul 2012, Jun 2013 and Mar 2015. Interestingly, further reduction in ApEn value $(0.29 - 0.40)$

302   was as well noticed during this period. Thus, during major geomagnetic storms, chaotic behaviour

303   and dynamical complexity subside significantly.

304   We display in Figure 6, the results of MLE and ApEn computation for the VB_s which has been

305   categorized according to the periods of minor, moderate and major geomagnetic storms. The

306   values of MLE (bar plot) were between 0.06 and 0.20 for VB_s. The result obtained indicate strong

307   chaotic behaviour with no significant difference in chaoticity during minor, moderate and major

308   geomagnetic storm. Similarly, the results obtained from computation of ApEn (stem plot) for VB_s

309   depict a minimum value of 0.60 and peak value of 0.87 as shown in Figure 6. The ApEn values of

310   VB_s indicates high dynamical complexity response with no significant difference during the

311   periods of the three categories of geomagnetic storm investigated.

312   The test for nonlinearity in the D_{st} signals during minor, moderate and major geomagnetic storms

313   was analyzed through the DVV analysis. Shown in Figure 9 is the DVV plot and DVV scatter plot

314   during minor geomagnetic storm for January 2009 and January 2014. We found that the DVV

315   plots during minor geomagnetic storms reveals a slight separation between the original and

316   surrogate data. Also, the DVV scatter plots shows a slight deviation from the bisector line between

317   the original and surrogate data which implies nonlinearity. Also, during moderate geomagnetic

318   storms, we notice that the DVV plot depicts a wide separation between the original and the

319   surrogate data. Also, a large deviation from the bisector line between the original and the surrogate

320   data was also noticed in the DVV scatter plot as shown in Figure (8) thus indicating nonlinearity.

321   In Figure (9), we display samples of DVV plot and DVV scatter plot during major geomagnetic

322   storm for Oct 2011 and Dec 2015. The original and the surrogate data showed a very large

323   separation in the DVV plot during major geomagnetic storm. While the DVV scatter plot depict

324   the greatest deviation from the bisector line between the original and the surrogate data which is

325   also an indication of nonlinearity. The DVV analysis of the VB_s time series during minor, moderate

326   and major geomagnetic storms shown in Figures (10-12) revealed a separation between the original

327   and surrogate data with no significant difference between the periods of minor, moderate and major

328   geomagnetic storm.

329   **4.0 Discussion of Results**

330   **4.1 The chaotic and dynamical complexity response in D_{st} at minor, moderate and major**

331   **geomagnetic storms**

332   Our result shows that the values of MLE for D_{st} during minor geomagnetic storm are higher,

333   indicating significant chaotic response during minor geomagnetic stormy periods (bar plot, Figure

334   5). This increase in chaotic behaviour for D_{st} signals during minor geomagnetic storms may be as

335   a result of asymmetry features in the longitudinal distribution of solar source region for the

336   Corotating Interaction Regions (CIR) signatures responsible for the development of geomagnetic

337   storms (Turner et al. 2006; Kozyra et al. 2006). CIR generated magnetic storms are generally

338   weaker than ICME/MC generated storms (Gonzalez et al., 1994; Tsurutani et al., 1995; Feldstein

339   et al., 2006; Richardson and Cane, 2011). Therefore, we suspect that the increase in chaotic

behaviour during minor geomagnetic storms is strongly associated with the asymmetry features in the longitudinal distribution of solar source region for the Corotating Interaction Regions (CIR) signatures. For most of these periods of moderate geomagnetic storms, the values of MLE decreases compared to minor geomagnetic storms. This revealed that as geomagnetic stormy events build up, the level of unpredictability and sensitive dependence on initial condition (chaos) begin to decrease (Lorentz, 1963; Stogaz, 1994). The chaotic behaviour during major geomagnetic storms decreases significantly compared with moderate geomagnetic storms. The reduction in chaotic response during moderate and its further declines at major geomagnetic storms may be attributed to the disturbance in the interplanetary medium driven by sheath preceding an interplanetary coronal mass ejection (ICME) or combination of the sheath and an ICME magnetic cloud (Echer et al., 2008; Tsurutani et al., 2003; Meng et al., 2019). Notably, the dynamics of the solar wind-magnetospheric interaction are dissipative chaotic in nature (Pavlos, 2012); and, the electrodynamics of the magnetosphere due to the flux of interplanetary electric fields had a significant impact on the state of the chaotic signatures. For instance, the observation of strong chaotic behaviour during minor geomagnetic storms suggests that the dynamics was characterized by a weak magnetospheric disturbance. While the reduction in chaotic behaviour at moderate and major geomagnetic storm period reveals the dynamical features with regards to when a strong magnetospheric disturbance begins to emerge. Therefore, our observation of chaotic signatures at different categories of geomagnetic storm has potential capacity to give useful diagnostic information about monitoring space weather events. It is important to note that the features of D_{st} chaotic behaviour at different categories of geomagnetic storm has not been reported in the literature. For example, previous study of Balasis et al. (2009, 2011) investigate dynamical complexity behaviour using different entropy measures and revealed the existence of low

363 dynamical complexity in the magnetospheric dynamics and attributed it to ongoing large

364 magnetospheric disturbance (major geomagnetic storm). The work of Balasis et al. (2009, 2011)

365 where certain dynamical characteristic evolved in the D_{st} signal was revealed was limited to one

366 year data (2001). It is worthy to note that the year 2001, according to sunspot variations is a period

367 of high solar activity during solar cycle 23. It is characterized by numerous and strong solar

368 eruptions that were followed by significant magnetic storm activities. This confirms that on most

369 of the days in year 2001, the geomagnetic activity is strongly associated with major geomagnetic

370 storms. The confirmation of low dynamical complexity response in the D_{st} signal during major

371 geomagnetic storms agree with our current study. However, the idea of comparing the dynamical

372 complexity behaviour at different categories of geomagnetic storms and reveal its chaotic features

373 was not reported. This is the major reason why our present investigation is crucial to the

374 understanding of the level of chaos and dynamical complexity involved during different categories

375 of geomagnetic storms. As an extension to the single-year investigation done by Balasis et al.

376 (2009, 2011) during a major geomagnetic storm, we further investigated nine years data of D_{st}

377 that covered minor, moderate and major geomagnetic storms (see Figure 5, stem plots) and

378 unveiled their dynamical complexity behaviour. During major geomagnetic stormy periods, we

379 found that the ApEn values decrease significantly, indicating reduction in the dynamical

380 complexity behaviour. This is in agreement with the low dynamical complexity reported by Balasis

381 et al. (2009, 2011) during a major geomagnetic period. Finally, based on the method of DVV

382 analysis, we found that test of nonlinearity in the D_{st} time series during major geomagnetic storms

383 reveals the strongest nonlinearity features.

384

385

4.2 The chaotic and dynamical complexity behaviour in the VB_s as input signals.

The results of the MLE values for VB_s revealed a strong chaotic behaviour during the three categories of geomagnetic storms. Comparing these MLE values during minor to those observed during moderate and major geomagnetic storms, the result obtained did not indicate any significant difference in chaoticity (bar plots, Figure 6). Also, the ApEn values of VB_s during the periods associated with minor, moderate and major geomagnetic storms revealed high dynamical complexity behaviour with no significant difference between the three categories of geomagnetic storms investigated. These observation of high chaotic and dynamical complexity behaviour in the dynamics of VB_s may be due to interplanetary discontinuities caused by the abrupt changes in the interplanetary magnetic field direction and plasma parameters (Tsurutani et al., 2010). Also, the indication of high chaotic and dynamical complexity behaviour in VB_s signifies that the solar wind electric field is stochastic in nature. The DVV analysis for VB_s revealed nonlinearity features with no significant difference between the minor, moderate and major geomagnetic storms. It is worth mentioning that the dynamical complexity behaviour for VB_s is different from what was observed for D_{st} time series data. For instance, our results for D_{st} times series revealed that the chaotic and dynamical complexity behaviour of the magnetospheric dynamics are high during minor geomagnetic storms, reduce at moderate geomagnetic storms and further decline during major geomagnetic storms. While the VB_s signal revealed a high chaotic and dynamical complexity behaviour at all the categories of geomagnetic storm period. Therefore, these dynamical features obtained in the VB_s as input signal and the D_{st} as the output in describing the magnetosphere as a non-autonomous system further support the finding of Donner et al. (2019) that found increased or not changed in dynamical complexity behaviour for VB_s and low dynamical complexity

408 behaviour during storm using recurrence method. Thus, suggesting that the magnetospheric

409 dynamics is nonlinear and the solar wind dynamics is consistently stochastic in nature.

410 **5.0 Conclusions**

411 This work has examined the magnetospheric chaos and dynamical complexity behaviour in the

412 disturbance storm time (D_{st}) and solar wind electric field (VB_s) as input during different categories

413 of geomagnetic storms. The chaotic and dynamical complexity behaviour at minor, moderate and

414 major geomagnetic storms for solar wind electric field (VB_s) as input and D_{st} as output of the

415 magnetospheric system were analyzed for the period of 9 years using nonlinear dynamics tools.

416 Our analysis has shown a noticeable trend of these nonlinear parameters (MLE and ApEn) and the

417 categories of geomagnetic storm (minor, moderate and major). The MLE and ApEn values of the

418 D_{st} have indicated that the chaotic and dynamical complexity behaviour are high during minor

419 geomagnetic storms, low during moderate geomagnetic storms and further reduced during major

420 geomagnetic storms. The values of MLE and ApEn obtained from VB_s indicate that chaotic and

421 dynamical complexity are high with no significant difference during the periods of minor,

422 moderate and major geomagnetic storms. Finally, the test for nonlinearity in the D_{st} time series

423 during major geomagnetic storms reveals the strongest nonlinearity features. Based on these

424 findings, the dynamical features obtained in the VB_s as input and D_{st} as output of the

425 magnetospheric system suggest that the magnetospheric dynamics is nonlinear and the solar wind

426 dynamics is consistently stochastic in nature.

427

428

429

7.0 Acknowledgement

The authors would like to acknowledge the World Data Centre for Geomagnetism, Kyoto, and the National Aeronautics and Space Administration, Space Physics Facility (NASA) for making the Dst data and solar wind plasma data available for research purpose. Also, the efforts of anonymous reviewers in ensuring that the quality of the work is enhanced are highly appreciated.

Declaration of Interest statement

The authors declare that there is no conflicts of interest.

References

Akasofu, S.I., (1964), The development of the auroral substorm. Planet. Space Sci., 12, 273-282, doi:10.1016/0032-0633(64)90151-5.

Baker, D.N., Klimas, A.J., (1990). The evolution of weak to strong geomagnetic activity: An interpretation in terms of deterministic chaos. J. GeoPhys. Res. Letts. Vol. 17, No. 1, PP. 41-44.

Balasis, G., Daglis, I.A., Anastasiadia, A., Eftaxias, K., (2011). Detection of dynamical complexity changes in Dst time series using entropy concepts and rescaled range analysis. W.Liu, M. Fujimoto (eds.), The Dynamics Magnetosphere, IAGA Special Sopron Book Series 3, doi: 10.1007/978-94-007-0501-2_12, Springer Science+Business Media B.V. 2011.

Balasis, G., I.A. Daglis, C. Papadimitriou, M. Kalimeri, A. Anastasiadis, K. Eftaxias (2009). Investigating dynamical complexity in the magnetosphere using various entropy measures, J.Geophys.Res., 114, A0006, doi: 10.1029/2008JA 014035.

450 Balasis, G., I.A. Daglis, P. Kapiris, M.Mandea, D. Vassilliadis, K. Eftaxias (2006). From pre-storm

451   activity to magnetic storms: a transition described in terms of fractal dynamics, Ann.Geophys.,

452   24, 3557-3567, www.ann-geophys.net/24/3557/2006.

453 Balikhin, M.A., Boynton, R.J., Billings, S.A., Gedalin, M., Ganushkina, N., Coca, D., (2010). Data

454   based quest for solar wind-magnetosphere coupling function, Geophys.Res.Lett, 37, L24107,

455   doi: 10.1029/2010GL045733.

456 Burton, R.K., McPherron, R.L., Russell, C.T., (1975). An empirical relationship between

457   interplanetary conditions and Dst. Journal of Geophysical Research, Vol.80, No.31.

458 Consolini, G., (2018), Emergence of dynamical complexity in the Earth's magnetosphere, Machine

459   learning techniques for space weather, PP. 177-202, doi: 10.1016/B978-0-12-811788-0.00007-

460   X

461 Cowley, S.W.H., (1995). The earth's magnetosphere: A brief beginner's guide, EOS

462   Trans.Am.GeoPhys.Union, 76, 525.

463 Dessler, A.J., Parker, E.N., (1959). Hydromagnetic theory of magnetic storm. J. GeoPhys. Res, 64,

464   PP 2239-2259.

465 Devi, S.P., Singh, S.B., Sharma, A.S., (2013). Deterministic dynamics of the magnetosphere:

466   results of the 0-1 test. Nonlin. Processes Geophys., 20, 11-18, 2013, www.nonlin-processes-

467   geophys.net/20/11/2013, doi: 10. 5194/npg-20-11-2013.

468 Donner, R.V., Balasis, G., Stolbova,V., Georgiou, M., Weiderman, M., Kurths, J. (2019).

469   Recurrence-based quantification of dynamical complexity in the earth's magnetosphere at

470  geospace storm time scales. Journal of Geophysical Research: Space Physics, 124, 90-108,

471  doi: 10.1029/2018JA025318.

472 Dungey, J.W., (1961). Interplanetary magnetic field and auroral zones. Phys.Rev.Lett., 6, 47, doi:

473  10.1103/PhysRevLett.6.47

474 Echer, E., Gonzalez, D., Alves, M.V., (2006). On the geomagnetic effects of solar wind

475  interplanetary magnetic structures. Space Weather, Vol.4, S06001,

476  doi:10.1029/2005SW000200.

477 Echer, E., Gonzalez, W.D., Tsurutani, B.T., Gonzalez, A. L. C., (2008), Interplanetary conditions

478  causing intense geomagnetic storms ($D_{st} \leq -100nT$) during solar cycle 23 (1996–2006), J.

479  Geophys. Res., 113, A05221, doi:10.1029/2007JA012744.

480 Feldstein, Y.I., Levitin, A.E., Kozyra, J.U., Tsurutani, B.T., Prigancova, L., Alperovich, L.,

481  Gonzalez, W.D., Mall, U., Alexeev, I.I., Gromava, L.I., Dremukhina, L.A., (2005). Self-

482  consistent modelling of the large-scale distortions in the geomagnetic field during the 24-27

483  September 1998 major geomagnetic storm. JGR, 110, A11214, doi: 10.1029/2004JA010584.

484 Feldstein, Y.I., Popov, V.A., Cumnock, J.A., Prigancova, A., Blomberg, L.G., Kozyra, J.U.,

485  Tsurutani, B.T., Gromova, L.I., Levitin, A.E., (2006). Auroral electrojets and boundaries of

486  plasma domains in the magnetosphere during magnetically disturbed intervals. Ann. Geophys.,

487  24, 2243-2276, www.ann-geophys.net/24/2243/2006/

488 Fraser, A.M., (1986). Using mutual information to estimate metric entropy, dimension and

489  entropies in chaotic system, Springer-Verlag, 1986, PP: 82-91.

490   Fraser, A.M., Swinney, H.L., (1986). Independent coordinates for strange attractors from mutual
491   information, Phys.Rev.A 33, 1134-1140.

492   Gautama, T., Mandic, D.P., Hulle, M.M.V., (2004). The delay vector variance method for detecting
493   determinism and nonlinearity in time series. Physica D, 190, 167-176, doi:
494   10.1016/j.physd.2003.11.001.

495   Gonzalez, W.D., Joselyn, J.A., Kamide, Y., Kroehl, H.W., Rostoker, G., Tsurutani, B.T.,
496   Vasyliunas, V.M., (1994). What is a geomagnetic storm? J. Geophys. Res.: Space Physics,
497   Vol. 99, issue A4, pg. 5771-5792, doi: 10.1029/93JA02867.

498   Gonzalez, W.D., Tsurutani, B.T., (1987). Criteria of interplanetary parameters causing intense
499   magnetic   storm $(Dst < -100nT)$.   Planetary   and   Space   Science,
500   https://ntrs.nasa.gov/search.jsp?R=198800068.

501   Gonzalez, W.D., Tsurutani, B.T., Gonalez, A.L.C., Smith, E.J., Tang, F., Akasofu, S.I., (1989).
502   JGR, 94, A7, 8835-8851, doi: 10.1029/JA094iA07p08835.

503   Hajra, R., Echer, E., Tsurutani, B.T., Gonazalez, W.D., (2013). Solar cycle dependence of High-
504   intensity Long-duration Continuous AE activity (HILDCAA) events, relativistic electron
505   predictors? (2013), JGR, Space Physics, 118, 5626-5638, doi: 10.1002/jgra.50530.

506   Hajra, R., Tsurutani, B.T., (2018), Interplanetary shocks inducing magnetospheric supersubstorms
507   (SML<-2500nT): unusual auroral morphologies and energy flow. The AstroPhysical Journal,
508   858:123(6pp), doi:10.3847/1538-4357/aabaed.

509   Horne, R.H., Glauert, S.A., Meredith, N.P., Boscher, D., Maget, V., Heynderickx, D., and Pitcford,

510   D. (2013). Space weather impacts on satellites and forecasting the Earths electron radiation

511   belts with SPACECAST. Space weather, **11,** 169 - 186

512   Imtiaz, A., (2010). Detection of nonlinearity and stochastic nature in time series by delay vector

513   variance method, International journal of Engineering & Technology, Vol. 10, No. 02.

514   Jaksic, V., Mandic, D.P., Ryan, K., Basu, B., Pakrashi V., (2016). A Comprehensive Study of the

515   Delay Vector Variance Method for Quantification of Nonlinearity in dynamical Systems.

516   *R.Soc.OpenSci.*, 2016: 3:150493, http://dx.doi.org/10.1098/rsos.150493.

517   Johnson, J.R., Wing, S., (2005), A solar cycle dependence of nonlinearity in magnetospheric

518   activity. J. Geophys. Res., 110, A04211, doi: 10.1029/2004JA010638.

519   Kannathal, N., M.L. Choo, U. R. Acharya, P. K. Sadasivan (2005). Entropies for detecting of

520   epilepsy in EEG, Computer Methods and Programs in Biomedicine (2005) 80, 187-194,

521   www.intl.elsevierhealth.com/journals/cmpb.

522   Kennel, M.B., R. Brown, H.D.I. Abarbanel (1992). Determining embedding dimension for phase-

523   space reconstruction using a geometrical construction, PHYSICAL REVIEW A, Volume 45,

524   Number 6.

525   Klimas, A.J., Vassilliasdis, D., Baker. D.N., Roberts, D.A., (1996). The organized nonlinear

526   dynamics of the magnetosphere. J. GeoPhys. Res. Vol.101, No. A6, PP 13089-13113.

527   Kozyra, J.U., Crowley, G., Emery, B.A., Fang, X., Maris, G., Mlynczak, M.G., Niciejewski, R.J.,

528   Palo, S.E., Paxton, L.J., Randall, C.E., Rong, P.P., Russell, J.M., Skinner, W., Solomon, S.C.,

529   Talaat, E.R., Wu, Q., Yee, J.H., (2006), Response of the Upper/Middle Atmosphere to Coronal

530   Holes and Powerful High-Speed Solar Wind Streams in 2003, Geophysical Monograph Series
531   167, 10.1029/167GM24.

532 Kugiumtzis, D., (1999). Test your surrogate before you test your nonlinearity, Phys. Rev. E, 60,
533   2808-2816.

534 Liou, K., Newell, P.T., Zhang, Y.-L., Paxton, L.J., (2013), Statistical comparison of isolated and
535   non-isolated auroral substorms. J. Geophys. Res. Space Physics, 118, 2466-2477, doi:
536   10.1002/jgra.50218.

537 Lorenz, E.N., (1963). Determining nonperiodic flow. J. Atmos.Sci.,20,130.

538 Love, J.J., Gannon, J.L. (2009). Revised Dst and the epicycles of magnetic disturbance: 1958-2007.
539   Ann.GeoPhys., 27, 3101-3131.

540 Mandic, D.P., Chen, M., Gautama, T., Van Hull, M.M., Constantinides, A., (2007). On the
541   Characterization of the Deterministic/Stochastic and Linear/Nonlinear Nature of Time Series.
542   *Proc.R.Soc*, 2008: A464, 1141-1160, doi: 10.1098/rspa. 2007.0154.

543 Mane, R., (1981). On the dimension of the compact invariant sets of certain nonlinear maps, D.Rand
544   and L.S.Young, eds, 1981.

545 Mckinley, R.A., Mclntire, L.K., Schmidt, R., Repperger, D.W., Caldwell, J.A., (2011). Evaluation
546   of Eye Metrics as a Detector of Fatigue. Human factor, 53 (4): 403-414, doi:
547   10.1177/0018720811411297.

548 Mendes, O., Domingues, M.O., Echer, E., Hajra, R., Menconi, V. E., (2017). Characterization of
549   high-intensity, long-duration continuous auroral activity (HILDCAA) events using recurrence

550   quantification analysis. Nonlin. Processes Geophys., 24, 407-417, doi: 10.5194/npg-24-407-

551   2017.

552   Mendes, O., Dominques, M.O., Echer, E., Hajra, R., Menconi, V.E., (2017), Characterization of

553   high-intnesity, long-duration continuous auroral activitity (HILDCAA) events using

554   recurrence quantification analysis. Nonlin. Processes Geophys.,24,407-417, doi:10.5194/npg-

555   24-407-2017.

556   Meng, X., Tsurutani, B. T., Mannucci, A. J. (2019). The solar and interplanetary causes of

557   superstorms (minimum Dst ≤ -250 nT) during the space age. Journal of Geophysical Research:

558   Space Physics, 124, 3926–3948. https://doi.org/10.1029/2018JA026425.

559   Millan, H., Gharbarian-Alavijeh, B., Garcia-Fornaris, I., (2010). Nonlinear dynamics of mean daily

560   temperature and dewpoint time series at Babolsar, Iran, 1961-2005. Elsevier, Atmospheric

561   Research 98 (2010) 89-101, doi: 10.1016/j.atmosres.2010.06.001.

562   Moore, C., Marchant, T., (2017). The approximate entropy concept extended to three dimensions

563   for calibrated, single parameter structural complexity interrogation of volumetric images.

564   Physics in Medicine & Biology, 62(15).

565   Oludehinwa, I.A., Olusola, O.I., Bolaji, O.S., Odeyemi, O.O., (2018). Investigation of nonlinearity

566   effect during storm time disturbance, Adv. Space. Res, 62 (2018) 440-456, doi:

567   10.1016/j.asr.2018.04.032.

568   Omkar, P.T., Verma, P.L., (2013). Solar features and solar wind plasma parameters with

569   geomagnetic storms during the period of 2002-2006. Indian Journal of Applied Research,

570   Vol.3, Issue.5, ISSN-2249-555X.

571 Pavlos, G.P., (1994). The magnetospheric chaos: a new point of view of the magnetospheric

572   dynamics. Historical evolution of magnetospheric chaos hypothesis the past two decades.

573   Conference Proceeding of the 2nd Panhellenic Symposium held in Democritus University of

574   Thrace, Greece, 26-29, April, edited 1994.

575 Pavlos, G.P., (2012). Magnetospheric dynamics and Chaos theory

576 Pavlos, G.P., Athanasiu, M.A., Diamantidis, D., Rigas, A.G., Sarri, E.T., (1999). Comments and

577   new results about the magnetospheric chaos hypothesis. Nonlinear Processes in Geophysics

578   (1999) 6: 99-127.

579 Pavlos, G.P., Rigas, A.G., Dialetis, D., Sarris, E.T., Karakatsanis, L.P., Tsonis, A.A., (1992).

580   Evidence of chaotic dynamics in the outer solar plasma and the earth magnetosphere. Chaotic

581   dynamics: Theory and Practice, Edited by T. Bountis, Plenum Press, New York, Page. 327-

582   339, doi:10.1007/978-1-4615-3464-8_30.

583 Pincus, S.M., (1991). Approximate entropy as a measure of system complexity, Proc.Natl.Acad.Sci.

584   USA, Vol.88, PP. 2297-2301.

585 Pincus, S.M., Goldberger, A.L., (1994). Physiological time series analysis: what does regularity

586   quantify, The American Journal of Physiology, 266 (4): 1643-1656.

587 Pincus, S.M., Kalman, E.K., (2004). Irregularity, volatility, risk, and financial market time series,

588   Proceedings of the National Academy of Sciences, 101 (38): 13709-13714, doi:

589   10.1073/pnas.0405168101.

590 Price, C.P., Prichard, D., Bischoff, J.E., (1994). Nonlinear input/output analysis of the auroral

591   electrojet index. Journal of Geophysical Research, Vol.99, No: A7, PP: 227-238.

592   Price,C.P., Prichard, D., (1993). The Non-linear response of the magnetosphere: 30 October, 1978.

593   Geophysical Research Letters, Vol.20.

594   Richardson, I.G.,   Cane, H.V., (2011), Geoeffectiveness (D_{st} and K_p) of interplanetary coronal

595   mass ejections during 1995-2009 and implication for storm forecasting, Space Weather, 9,

596   S07005, doi:10.1029/2011SW000670.

597   Russell, C.T., (2001). Solar wind and Interplanetary Magnetic Field: A Tutorial. Space Weather,

598   Geophysical Monograph 125, Page: 73-89.

599   Russell, C.T., McPherron, R.L., Burton, R.K. (1974). On the cause of geomagnetic storms,

600   J.GeoPhys.Res., 79, 1105-1109.

601   Shujuan G., Weidong, Z., (2010). Nonlinear feature comparison of EEG using correlation

602   dimension and approximate entropy, 3rd international conference on biomedical engineering

603   and informatics.

604   Strogatz, S.H., (1994), Nonlinear dynamics and chaos with Application to physics, Biology,

605   chemistry and Engineering, New York, John Wiley & Sons.

606   Sugiura, M. (1964). Hourly Values of equatorial Dst for the IGY, Ann.Int. GeoPhys. Year, 35, 9-

607   45.

608   Takens, F., (1981). Detecting Strange Attractors in Turbulence in Dynamical Systems, D.*Rand &*

609   *L.Young Eds*, 1981: 898, 366-381.

610   Theiler, J., Eubank, S., Longtin, A., Galdrikian, B., Farmer, J.D., (1992), Testing for nonlinearity

611   in time series: The method of surrogate data, Physica D, 58, 77.

612 Tsurutani, B.T., Gonazalez, W.D., (1987), The cause of High-intensity Long duration Continuous

613   AE activity (HILDCAAs): Interplanetary Alfven trains. Planet. Space Sci., 35, 4, 405-412, doi:

614   10.1016/0032-0633(87)90097-3.

615 Tsurutani, B.T., Gonzalez, A.L.C., Tang, F., Arballo, J.K., Okada, M., (1995), Interplanetary origin

616   of geomagnetic activity in the declining phase of the solar cycle. JGR, 100, A11, 717-733,

617   95JA01476.

618 Tsurutani, B.T., Gonzalez, W. D., Tang, F., Akasofu, S.I., Smith, E.J., (1988), Origin of

619   Interplanetary Southward Magnetic Fields Responsible for Major Magnetic Storms Near Solar

620   Maximum (1978-1979), Journal of Geophysical Research, Vol. 93, No. A8, Pages 8519-8531,

621   Paper number 7A9404, 0148-0227/88/007 A-9404$05.00.

622 Tsurutani, B.T., Gonzalez, W.D., Lakhina, G.S. Alex, S., (2003). The extreme magnetic storm of

623   1-2 September 1859, J. Geophys. Res. 108(A7), doi: 10.1029/2002JA009504.

624   Tsurutani, B.T., Hajra, R., (2021). The interplanetary and magnetospheric causes of

625   geomagnetically induced currents (GICs) >10A in the Mantsala finland Pipeline: 1999

626   through 2019. J. Space Weather Space Clim, 11, 23, doi: 10.1051/swsc/2021001.

627 Tsurutani, B.T., Lakhina, G.S., Hajra, R., (2020), The physics of space weather/solar-terrestrial

628   physics (STP): what we know now and what the current and future challenges are, Nonlin.

629   Processes Geophys., 27, 75–119, doi:10.5194/npg-27-75-2020.

630 Tsurutani, B.T., Lakhina, G.S., Verkhoglyadova, O.P., Gonzalez, W.D., Echer, E., Guarnieri, F.L.,

631   (2010). A review of interplanertary discontinuities and their geomagnetic effects. Journal of

632   Atmospheric and Solar-Terrestrial Physics, doi: 10.1016/j.jastp.2010.04.001.

633 Tsurutani, B.T., Sugiura, M., Iyemori, T., Goldstein, B.E., Gonazalez, W.D., Akasofu, S.I., Smith,

634   E.J., (1990). The nonlinear response of AE to the IMF Bs driver: A spectral break at 5 hours.

635   Geophysical Research Letters, Vol.17, No.3., Pages: 279-283.

636 Tsutomu, N., (2002). Geomagnetic storms. Journal of communications Research Laboratory, Vol.

637   49, No.3.

638 Turner, N.E., Mitchell, E.J., Knipp, D.J., Emery, B.A., (2006), Energetics of magnetic storms

639   driven by corotating interaction regions: a study of geoeffectiveness, Geophysical Monograph

640   Series 167, 10.1029/167GM11.

641 Unikrishnan, K., (2008). Comparison of chaotic aspect of magnetosphere under various physical

642   conditions using AE index time series. Ann. Geophys., 26, 941-953, www.ann-

643   geophys.net/26/941/2008.

644 Unikrishnan, K., Ravindran, S., (2010). A study on chaotic behaviour of equatorial/low latitude

645   ionosphere over indian sub-continent, using GPS-TEC time series, J. Atmos. Sol. Ter. Phys.,

646   72, 1080-1089.

647 Valdivia, J.A., Rogan, J., Munoz, V., Gomberoff, L., Klimas, A., Vassilliasdis, D., Uritsky, V.,

648   Sharma, S., Toledo, B., Wastaviono, L. (2005). The magnetosphere as a complex system. Adv.

649   Space. Res, 35, 961-971.

650 Valdivia, J.A., Sharma, A.S., Papadopoulos, K., (1996). Prediction of magnetic storms by nonlinear

651   models. Geophysical Research Letters, 23(21), 2899-2902, doi: 10.1029/96GL02828.

652 Vassiliadis, D., (2006). Systems theory for geospace plasma dynamics, Rev.Geophys., 44, RG2002,

653   doi: 10.1029/2004RG000161.

654 Vassiliadis, D., Klimas, A.J., Valdivia, J.A., Baker, D.N., (1999). The geomagnetic response as a

655 function of storm phase and amplitude and solar wind electric field. Journal of Geophysical

656 Research, 104(A11), 24957-24976, doi: 10.1029/1999JA900185.

657 Vassilliadis, D., Sharma, A.S., Papadopoulos, K., (1991). Lyapunov exponent of magnetospheric

658 activity from AL time series. J. GeoPhys. Letts, Vol. 18, No.8, PP. 1643-1646.

659 Vassilliadis, D.V., Sharma, A.S., Eastman, T.E., Papadopoulou, K., (1990). Low-dimensional

660 chaos in magnetospheric activity from AE time series. J. GeoPhys.Res.Lett, 17, 1841-1844.

661 Wallot, S., Monster, D., (2018). Calculation of Average Mutual Information (AMI) and False

662 Nearest Neigbhours (FNN) for the estimation of embedding parameters of multidimensional

663 time series in MATLAB. Front. Physchol. 9:1679, doi: 10.3389/fpsyg.2018.01679.

664 Watari, S., (2017). Geomagnetic storms of cycle 24 and their solar sources, Earth, Planets and

665 Space, PP: 69:70, doi: 10.1186/s40623-017-0653-z.

666 Wolf, A., Swift, J. B., Swinney, H. L., and Vastano, J. A. (1985). Determining Lyapunov exponents

667 from a time series, *Physica D*, *16*, 285–317, doi:10.1016/0167-2789(85)90011-9.

668 Zhang, J., Dere, K.P., Howard, R.A., Bothmer, V., (2002), Identification of solar sources of major

669 geomagnetic storms between 1996 and 2000. Astrophysical Journal, 582:520-53.

670
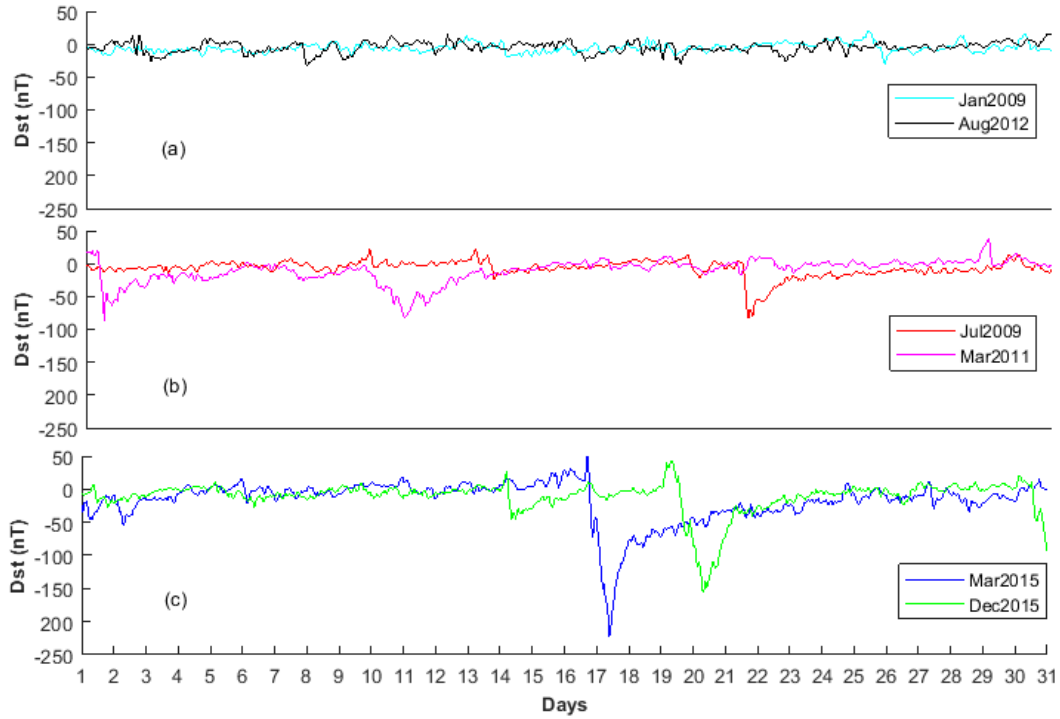
Figure 1: Samples of D_{st} signals classified as (a) Minor, (b) Moderate and (c) Major geomagnetic
storm

673
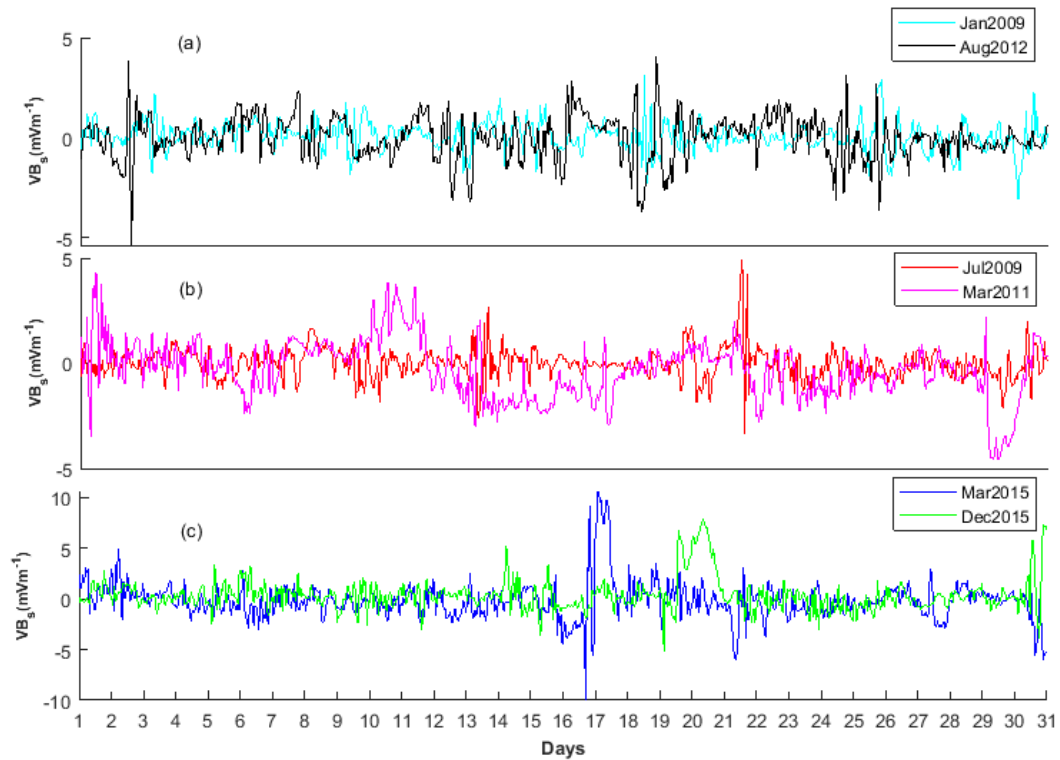
Figure 2: Samples of solar wind electric fields (VB_s) during (a) Minor, (b) Moderate and (c) Major
geomagnetic storm.

676
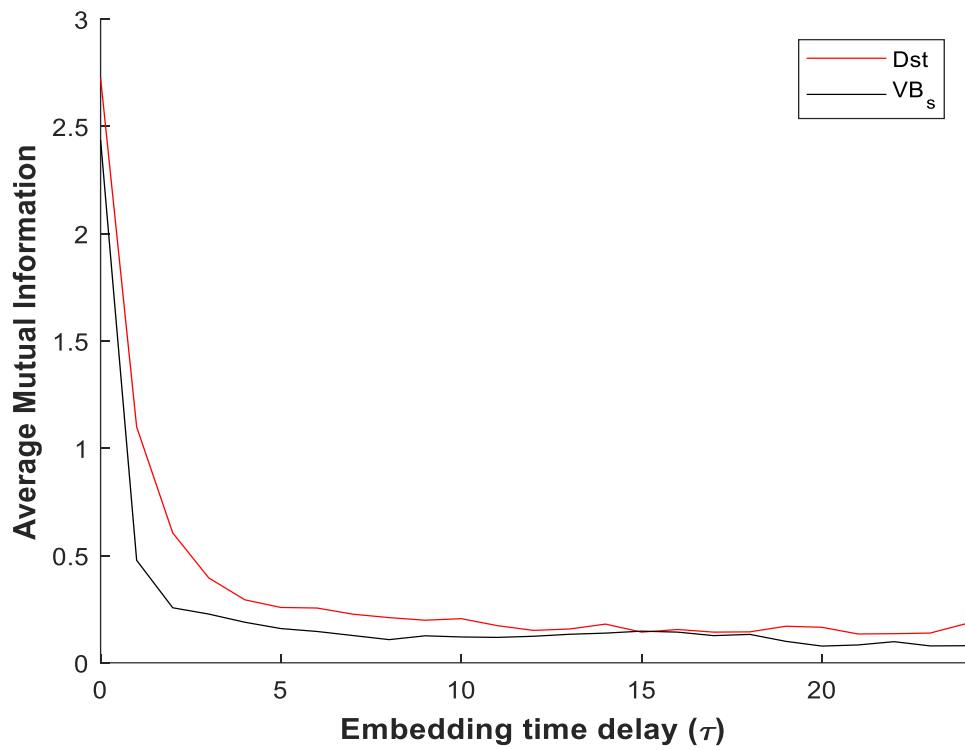
677

678   Figure 3: The plot Average Mutual Information against embedding time delay (τ)
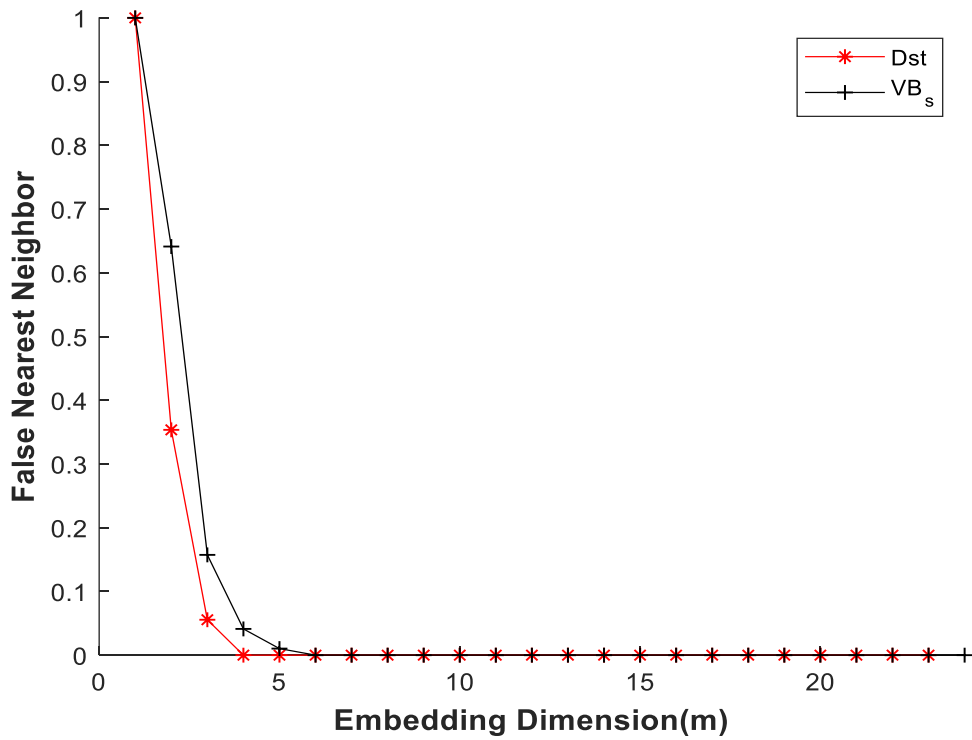
679

680   Figure 4: The plot of Percentage of False Nearest Neighbors against embedding dimension (m)

681
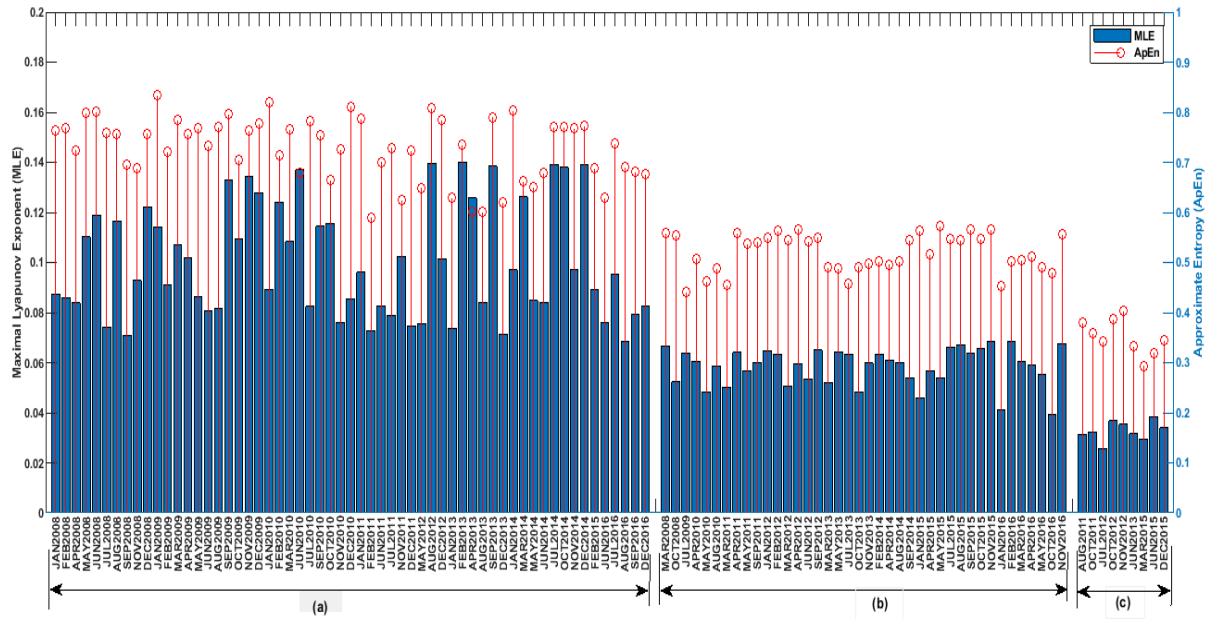
Figure 5: The MLE (bar plot) and ApEn (stem plot) of D_{st} at: (a) Minor, (b) Moderate and (c) Major geomagnetic storm.

691
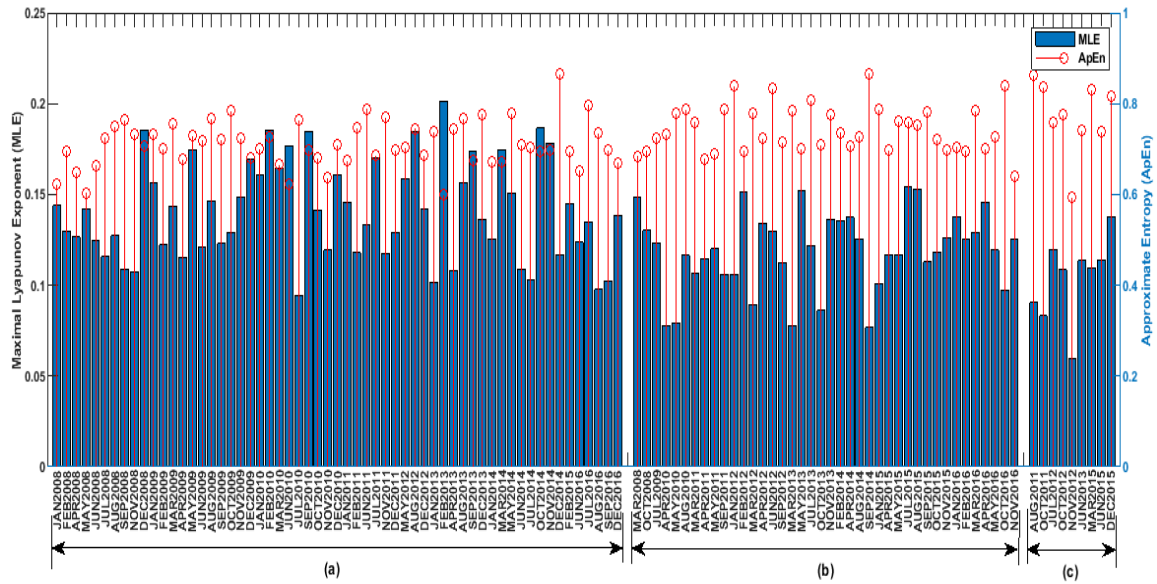
Figure 6: The MLE (bar plot) and ApEn (stem plot) of solar wind electric field (VB_s) during: (a)
Minor, (b) Moderate and (c) Major geomagnetic storm.

694

695

696

697

698

699

700

701

702

703

704

705

706

707
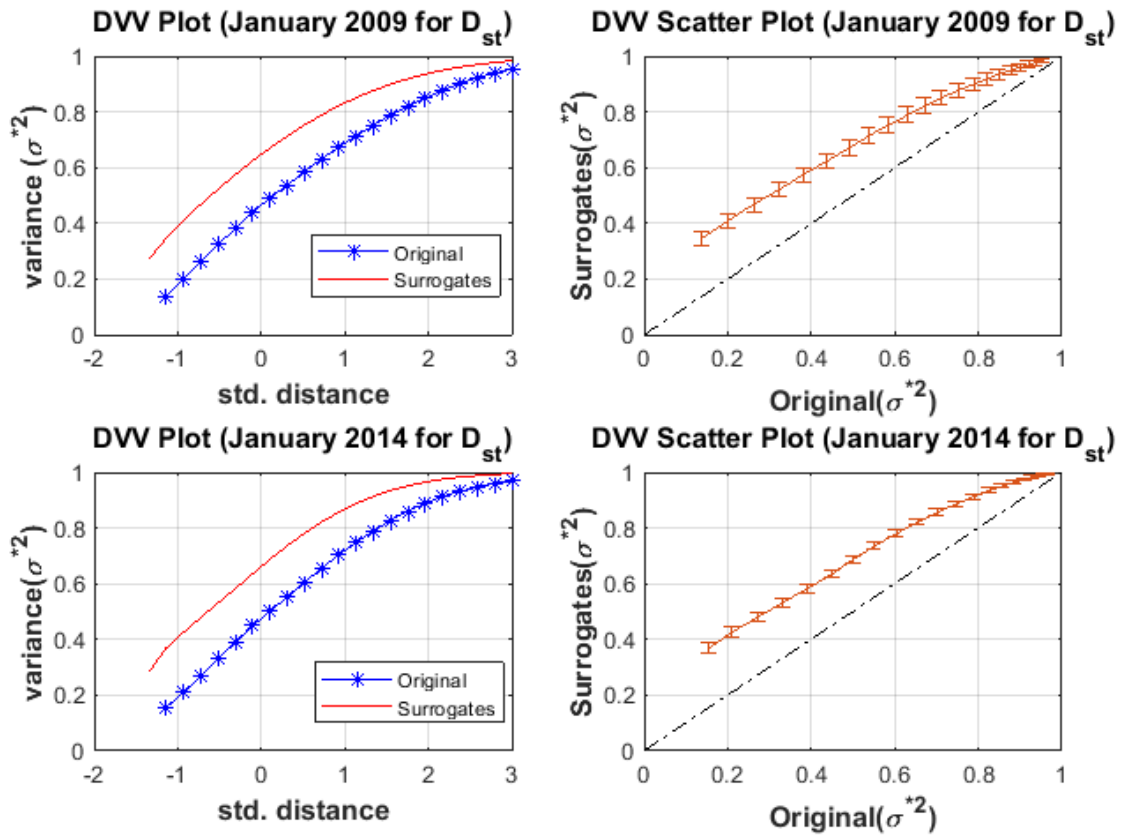
Figure 7: The DVV plot and Scatter plot for D_{st} during minor geomagnetic storm for January 2009 and January 2014.
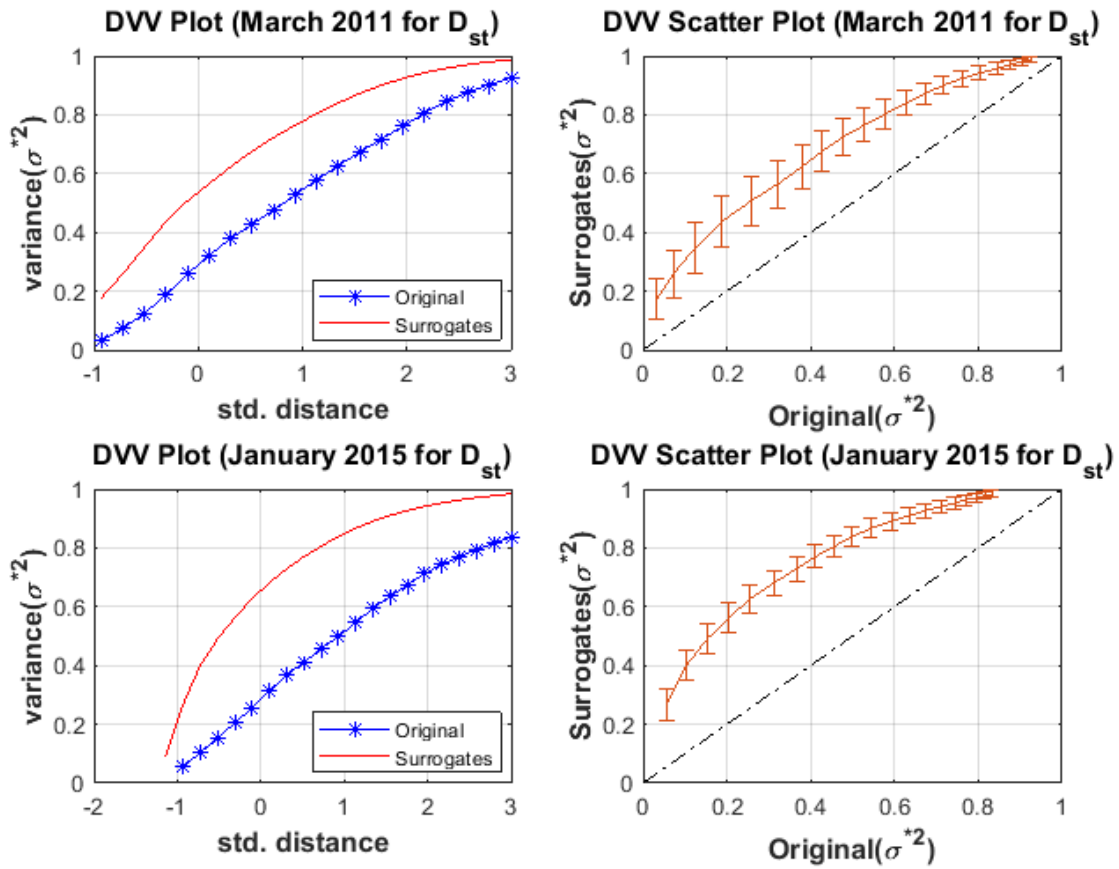
710

711

712 Figure 8: The DVV plot and Scatter plot for D_{st} during moderate geomagnetic storm for March
713 2011 and January 2015.

714

715
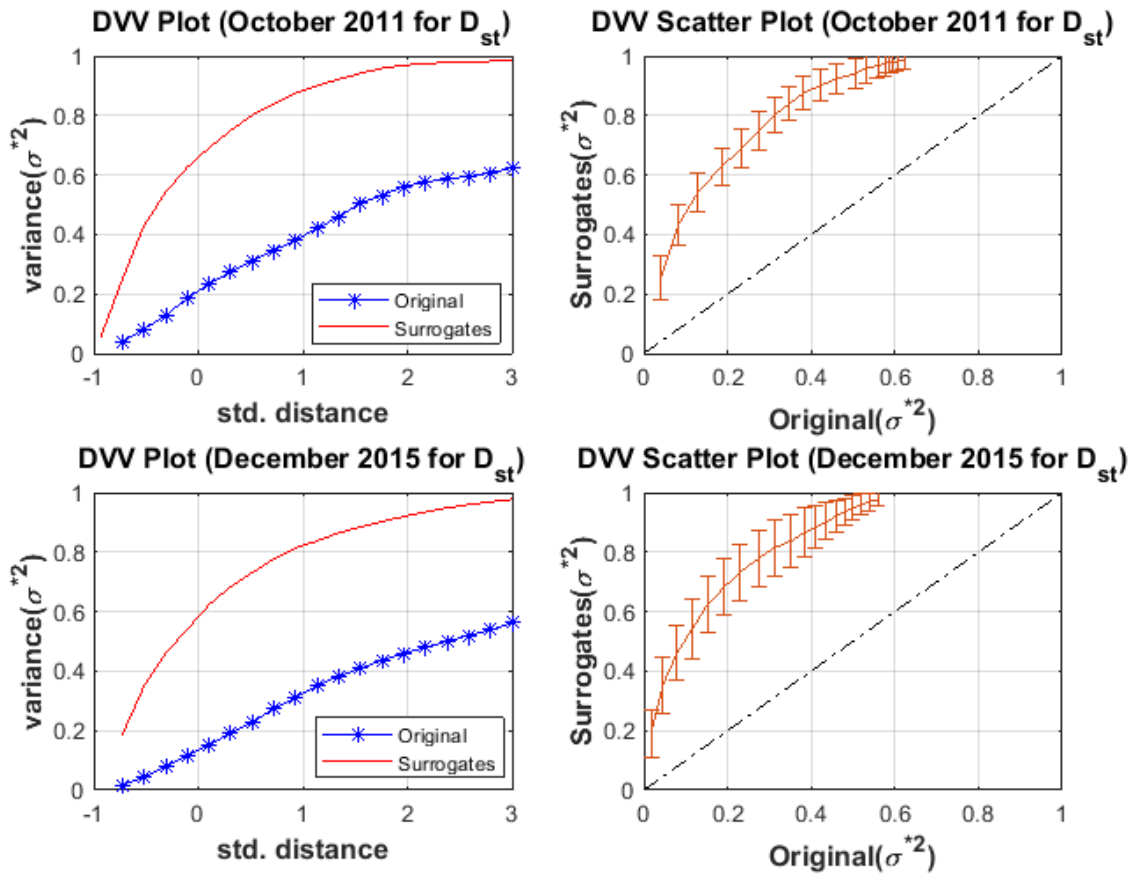
Figure 9: The DVV plot and Scatter plot for D_{st} during major geomagnetic storm for October
2011 and December 2015.

719
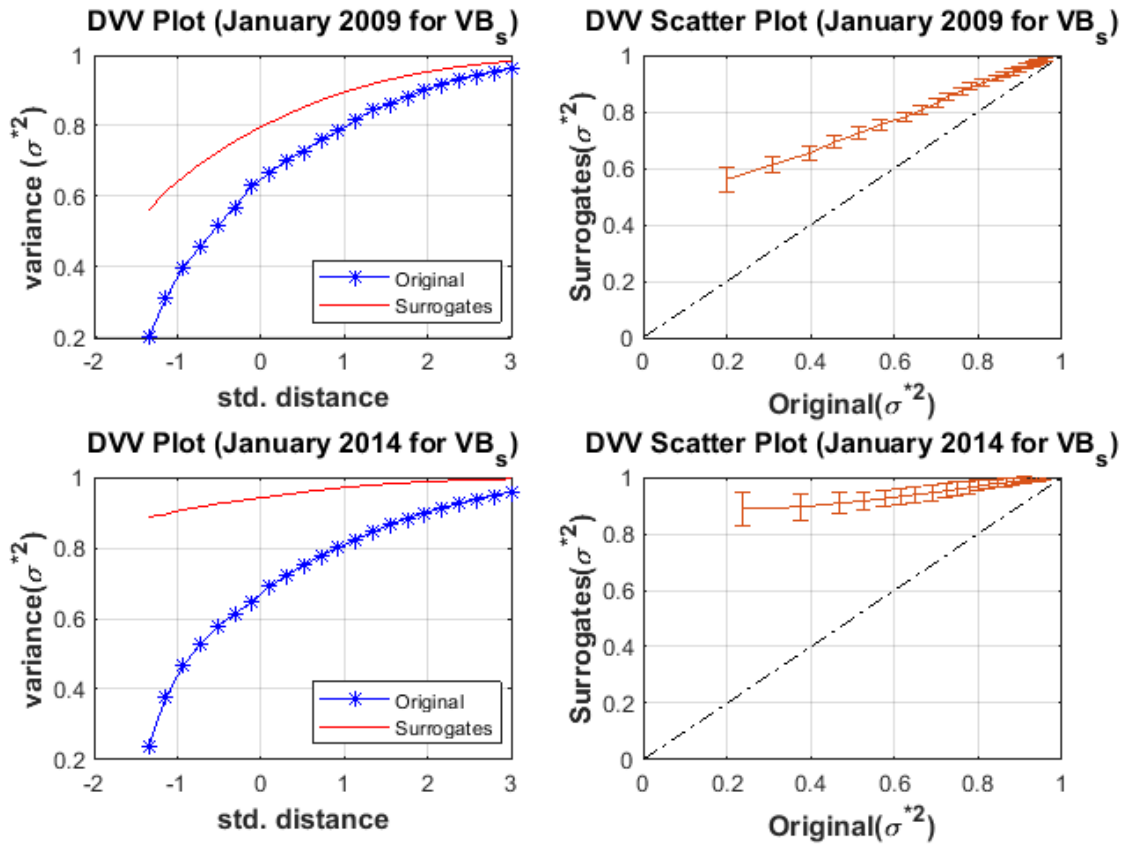
Figure 10: The DVV plot and Scatter plot for VB_s during minor geomagnetic storm for January
2009 and January 2014.

721

722

723
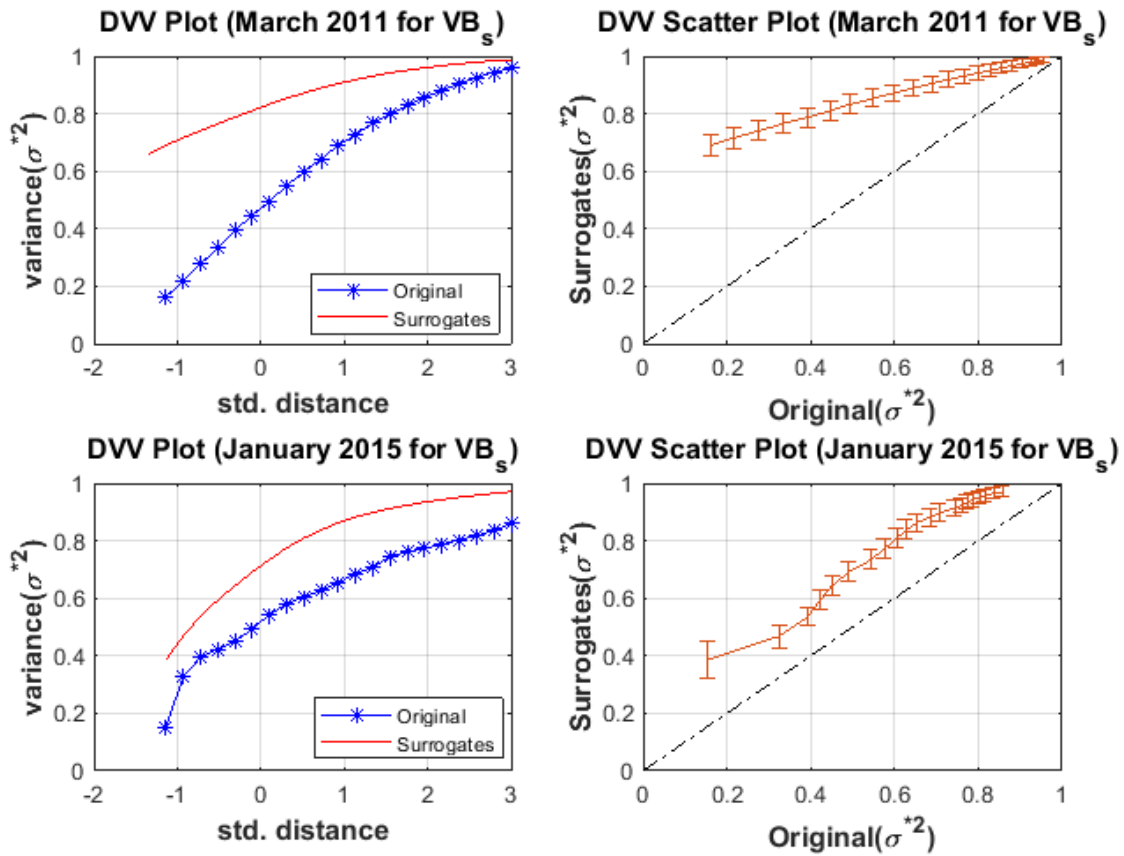
724

725   Figure 11: The DVV plot and Scatter plot for VB_S during moderate geomagnetic storm for March
726   2011 and January 2015.

727

728
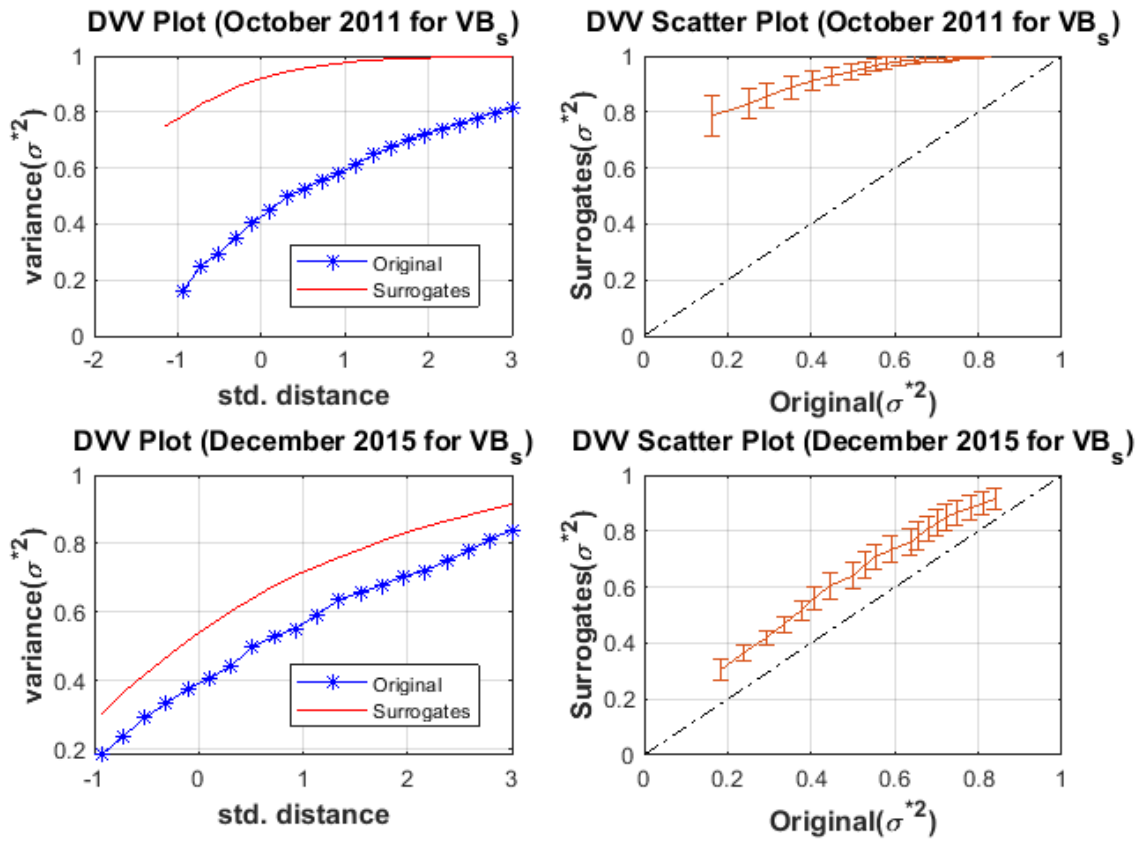
729

730   Figure 12: The DVV plot and Scatter plot for VB_s during major geomagnetic storm for October
731   2011 and December 2015.

732

733

734